Lezhennikova, Kseniia; Simovski, C.; Abdeddaim, R.; Balafendiev, R.; Glybovski, S.

Extending a Birdcage Coil for Magnetic Resonance Imaging of a Human Head with an Artificial Magnetic Shield

Published in:
Photonics and Nanostructures: Fundamentals and Applications

DOI:
10.1016/j.photonics.2020.100890

Published: 01/02/2021

Document Version
Peer-reviewed accepted author manuscript, also known as Final accepted manuscript or Post-print

Please cite the original version:
Lezhennikova, K., Simovski, C., Abdeddaim, R., Balafendiev, R., & Glybovski, S. (2021). Extending a Birdcage Coil for Magnetic Resonance Imaging of a Human Head with an Artificial Magnetic Shield. *Photonics and Nanostructures: Fundamentals and Applications*, *43*, Article 100890. https://doi.org/10.1016/j.photonics.2020.100890

Journal Pre-proof

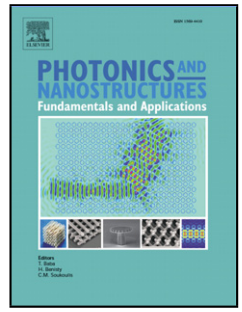

Extending a Birdcage Coil for Magnetic Resonance Imaging of a Human Head with an Artificial Magnetic Shield

K. Lezhennikova, C. Simovski, R. Abdeddaim, R. Balafendiev, S. Glybovski

PII: S1569-4410(20)30218-2

DOI: https://doi.org/10.1016/j.photonics.2020.100890

Reference: PNFA 100890

To appear in: *Photonics and Nanostructures - Fundamentals and Applications*

Received Date: 2 November 2020

Revised Date: 20 November 2020

Accepted Date: 8 December 2020

Extending a Birdcage Coil for Magnetic Resonance Imaging of a Human Head with an Artificial Magnetic Shield

K. Lezhennikova[a,*], C. Simovski[a,b], R. Abdeddaim[c], R. Balafendiev[a], S. Glybovski[a]

[a]Department of Physics and Engineering, ITMO University, St.Petersburg, Russia
[b]Department of Electronics and Nanoengineering, Aalto University, Aalto, Finland
[c]Aix Marseille Université, CNRS, Centrale Marseille, Institut Fresnel, Institut Marseille Imaging, Marseille, France

Abstract

In magnetic resonance imaging a birdcage coil is the most commonly used volumetric resonator creating highly homogeneous radiofrequency magnetic field in a conductive sample. An artificial magnetic radiofrequency shield was recently shown to improve the magnetic field amplitude per unit power (transmit efficiency) of a preclinical birdcage coil by reducing the intrinsic losses in the coil and increasing power absorbed by the sample. In this paper, we propose a new application of an artificial shield in clinical MRI. Thanks to the proposed artificial shield a birdcage coil for human brain imaging operating at 300 MHz (Larmor frequency of protons at static fields of 7 T) can be expanded to increase free space. As a result, the coil becomes more comfortable for the patient and keeping comparable transmit efficiency. The same extended coil with a conventional copper shield would have at least 10% lower efficiency. The proposed artificial shield is implemented as an annular-ring cavity-backed slot in a copper cylinder that tightly surrounds the birdcage. To demonstrate the effect, radiofrequency magnetic field and specific absorption rate distributions were compared numerically and experimentally for the initial and extended coils with different shields.

Keywords: ultra-high field MRI, magnetic shield, human head MRI, birdcage coil

1. Introduction

Magnetic resonance imaging (MRI) [1] is one of the most informative and safe methods of non-invasive diagnosis of diseases and one of the most important tools for biomedical research. In any MR scanner, radio-frequency (RF) coils are responsible for the excitation of spins (mainly of protons) in an investigated sample with RF pulses and for the detection of their resonance response [2]. The most frequently used transmit RF coil in MRI is a birdcage coil [3] providing at low frequencies a homogeneous magnetic field in the region of interest (ROI). MRI actively develops towards higher resolution and shorter scan time due to the transfer of clinical MRI to higher fields [4]. Ultra-high-field (UHF) MR scanners have already demonstrated superior capabilities providing a new level of medical diagnostics [5, 6]. Though at the moment, most of the available MRI scanners in hospitals worldwide operate with static fields from 1.5 to 3 T (high field with Larmor frequencies from 64 to 128 MHz), research scanners for the whole human body have reached the field of 7-10.5 T. Currently the new research direction is to adapt 7 T to the clinical use [7]. Recently 7 T MRI was certified for clinical applications but only with very limited hardware operation due to specific problems of Larmor frequencies elevated to 300 MHz such as high and hardly predictable RF power deposition of body tissues, and visible inhomogeneity of images [8]. To generate the most uniform magnetic field in the head in UHF MRI local arrays for parallel transmission typically composed of loop or dipole antennas are used [9, 10, 11]. This approach, however, requires multi-channel transmit systems, that are expensive and difficult to operate with. Therefore, their use is limited, and so far birdcage coils remain the only possible solution for clinical MRI of a human head at 7 T.

The most important specifications for transmit RF coils are transmit efficiency, and specific energy absorption rate (SAR). The transmit efficiency is defined as the amplitude of the transmit magnetic field with right-hand circular polarization created by the coil in the ROI (B_1^+) for a given power accepted by the coil from a transmitter. For all calculations in this paper the given power is 0.5 W and all B_1^+ distributions are representing the efficiency levels measured in uT. SAR is defined as the RF power absorbed per unit of mass of the sample (W/kg). Coils for brain imaging are usually placed as close as possible to the patient's head to maximize the transmit efficiency. Tight-fitting coils despite having better efficiency create high hotspots of SAR, which may decrease the ratio of $B_1^+/\sqrt{\text{SAR}}$ (i.e., the safety excitation efficiency (SEE)) [12]. Also, a tight coil is less comfortable for the patient and provides limited access to the ROI during the scan time. Finally, in ultra-high-field MRI, a combination of a transmit birdcage

*Corresponding author
Email address: ksenia.lezhennikova@metalab.ifmo.ru (K. Lezhennikova)

coil and an array of receive loops is used to benefit from the improved signal-to-noise ratio (SNR) while using only one transmit channel. In this scenario, the local receive array occupies the space between the head and conductors of the birdcage. As a result, the comfort of patients is further decreased. To increase the free space one could enlarge the radius of the birdcage coil. However, in this case, the transmit power drops down due to dissipation inside the coil and to undesirable radiation. In this case, the coil becomes insufficiently loaded meaning that not all the transmit power goes to the sample, which, as well known [13], limits the transmit efficiency.

Another factor that affects the transmit efficiency of the birdcage coil is the presence of a shield. Usually, such coils are shielded from the gradient system with a copper foil or grid to reduce radiation losses and make the performance stable [14]. As a result, both the electric and magnetic fields noticeably grow in the gap between the coil and the shield while reducing at the sample position at the center [15]. This effect occurs due to a negligible surface impedance of a metal shield. This boundary condition enforces an almost zero tangential electric field leading to out-of-phase reflection of electromagnetic waves created by the birdcage coil. In turn, this causes a strong destructive interference of the initial field and the reflected one.

There is, however, a perfectly reflecting magnetic RF shield, that on the contrary, reflects electromagnetic waves in phase. It can be represented as a surface with a tangential magnetic field component vanishing due to an infinite surface impedance. This property is provided by a boundary of a so-called perfect magnetic conductor (PMC). However, natural magnetic conductors do not exist and can be only approximated in a narrow frequency range with resonant periodic structures called artificial magnetic conductors (AMCs). The latter exhibit very high surface impedance (much higher than a free-space wave impedance) at the resonance of their unit cells. The impedance of such structures, also known as high-impedance surfaces (HISs) is frequency-dependent and almost reactive (with a dominant imaginary part) [16]. HISs are widely used in antenna design as shields that can be placed much closer than the quarter wavelength to a dipole or microstrip radiators still providing in-phase reflection [17, 18]. One of the first structures providing reflecting plane waves in-phase is a corrugated wall [19]. The top surface of an array of periodic straight grooves in metal operates as a HIS for TM polarization of an incident wave in a wide range of incidence angles. Since the grooves must be of the quarter-wave depth, to be compact each groove should be filled with a high-permittivity material. Another approach is to use low-profile mushroom surfaces proposed in [17]. Mushroom surfaces are produced as thin grounded slabs with patches connected through vias to the ground. The operational principles and different realizations of HISs were reviewed e.g. in. [16]

The idea of using a HIS to improve the performance of RF coils in MRI was earlier suggested in the literature by several authors. A HIS has been applied to individually driven dipole elements of a head array coil for parallel transmission in brain imaging [20] and to a surface-loop coil for breast imaging in a 7-T MRI system [21]. In both cases, the improvement of the RF-field distribution in a phantom (a conducting sample mimicking electric properties of body tissues) and increased efficiency were observed. However, the study of using HISs in the most popular transmit coils for MRI, i.e. birdcage coils has been studied only recently. In [22] the authors first suggested using an artificial magnetic shield consisting of split-ring resonators with a birdcage coil for full-body MRI to reduce the hotspots SAR. It was shown that the structure in [22] provides more homogeneous B_1 field and lower electric field. In [23] it was shown that the artificial magnetic shield realized as a miniaturized corrugated structure when used as a shied increases the efficiency of the preclinical birdcage coil and this improvement depends on the size of a conducting sample. The efficiency gain of 13% was numerically and experimentally demonstrated for MRI at 7 T for the artificial magnetic shield over a conventional copper shield. At the same time, the shape of the RF magnetic field pattern in the sample was not distorted in comparison to the copper shield. As a result, by using a corrugated shield one can improve the signal-to-noise ratio when using the same coil for the reception, but with the same homogeneity. However, since a small preclinical birdcage was considered, no analysis of SAR was made in [23].

In this paper, we extend the approach of using HISs to improve the transmit efficiency of the birdcage coil to human MRI by solving the following problem. The tight-fit birdcage coil for human brain imaging maximizes its transmit efficiency when properly loaded, that is, most of the transmit power is dissipated in the sample with minimum possible to be dissipated in the coil or radiated. We numerically and experimentally demonstrate that thanks to using a shield with a resonant cavity-backed annular-ring slot it is possible to extend the volume of a birdcage coil without a sugnificant degradation of its efficiency. The coil, therefore, becomes much more comfortable for a patient due to larger free space while having lower SAR and comparable efficiency as the initial tight-fit configuration.

2. METHODS

2.1. Numerical simulations

All numerical simulations were done using CST Microwave Studio 2019 software. A typical high-pass birdcage coil for brain imaging at 7 T (operational frequency of 300 MHz is Larmor frequency of protons) surrounded by a cylindrical copper shield was chosen as a reference and the initial configuration to be extended. The radius of the coil was $R_{\mathrm{reference}} = 150$ mm and shield radius $R_{\mathrm{reference\ shield}} = 160$ mm, the width of the rungs was

$W = 20$mm. As an extended coil, we considered a birdcage coil with the radius $R_{\text{extended}} = 200$ mm, and the same number of rungs as the reference coil, the width of the rungs was $W = 40$ mm, and the shield radius was $R_{\text{extended shield}} = 210$ mm. The width of the rungs of the extended coil was doubled with respect to the corresponding width of the initial coil to avoid small values of end-ring capacitance and therefore, to improve reproducibility of tuning in the experiment. The effect of the width of the rung width on the efficiency of coil was numerically estimated to be less than 1%. Therefore, it is correct to compare both coils despite of different widths. The above parameters are explained in Fig 1. Then for this extended coil, the cylindrical copper shield was replaced with a cylindrical PMC shield modeled as a slab of PMC with frequency-independent properties, and then the PMC shield was replaced by a HIS shield. The HIS shield was described with a frequency-dependent surface impedance. The dispersion corresponded to extracted resonant surface impedance of a real flat corrugated structure with a depth of corrugations 15 mm, relative permittivity $\varepsilon_{\text{r}} = 140$ of the dielectric filling the corrugations. After numerical simulations of the structure with periodic boundary conditions, the dispersive surface impedance was extracted and then applied to a uniform and isotropic boundary condition at the cylinder of the HIS shield surrounding the extended birdcage coil. The calculated frequency dependence of the real and imaginary parts of the surface impedance and the geometry of the corrugated structure are shown in Fig.2. The resonance of the surface impedance is observed at 530 MHz. But the birdcage and HIS shield when combined behave as coupled resonators. Due to this coupling the common mode was shifted down to 300 MHz despite that both the fundamental modes of the birdcage and HIS resonated individually at higher frequencies. In particular the fundamental mode of the birdcage couples to the fundamental mode of the HIS shield. The birdcage end-ring capacitors are tuned after combining so that the common coupled mode of this system resonates at the Larmor frequency of 7 T (300 MHz). CST models of the above-described coils are shown in Fig. 1. The results of Fig1 (d) demonstrate the field modification due to HIS under the assumption of a scalar and local surface impedance shown in Fig. 2, which is an approximate method. Indeed the birdcage creates evanescent modes that interact with the model HIS not like with the realistic corrugated structure depicted in Fig. 1. However, the effect of HIS on the field in the center of the phantom is mainly due to propagating waves and it is the same as for the corrugated structure. Therefore, the calculated efficiency in the center is a correct estimation for the constructive interference due to a shield.

Despite a cylindrical corrugated structure filled with high-permittivity dielectric could behave as an artificial a magnetic RF shield, this structure would be very heavy and expensive for the considered sizes. Therefore we proposed a simplified version of the shield, which, as we show, provides a similar effect to the birdcage coil while being composed only of metal parts. The simplified resonator contains a single annular-ring slot in copper cylinder and backed by a coaxial cavity. The slot of the 1-mm width is cut around the whole circumference of the cylinder in its middle transverse plane. The slot with the outer coaxial cavity as shown in Fig. 3. In fact, the slot connects the inner cylindrical volume with the outer coaxial cavity. At the resonance of the outer cavity, the slot behaves as a ring of magnetic current flowing around the circumference of the cylindrical shield. As for the HIS shield, this single-slot resonator supports a fundamental mode which couples to the fundamental mode of a birdcage coil placed inside the resonator. The common mode of the system, in this case, resonates at the Larmor frequency if the slot resonator alone resonates at 590 MHz (which is close to the required tuning frequency of an idealized HIS shield). To achieve this tuning condition, the main parameter, the axial length of the outer coaxial cavity L_{res} should be equal to 80 mm, while for compactness the radial width h_{res} of the cavity is limited to 23 mm. The CST model of the birdcage coil with the resonator is shown in Fig. 3.

All birdcage coils (either with a reference or extended size) were composed of $N = 12$ copper rungs with the length $L = 180$ mm and were surrounded by a cylindrical shield, at the radial distance $g = 10$ mm from the rungs. In all considered cases two discrete ports were placed parallel to the end-ring capacitors 90 degrees apart and fed in the quadrature regime to maximize the transmit efficiency of these coils. The maximum of the local SAR averaged for 10g were calculated for the given accepted power 0.25 W per port (0.5 W in total).

At the first step, we investigated the transmit efficiency of the described above birdcage coils in the case of a homogeneous phantom of the human head with the properties $\varepsilon_r = 50$, $\sigma = 0.657$ S/m [24]. At the next step, we numerically simulated the reference and extended coils with a copper shield and the extended coil with the resonator. We investigated the transmit efficiency and local SAR using a virtual family multi-tissue model "Duke" [25] for the human head situated in the middle of the birdcage. To compare the performance of the coils for different head sizes, the voxel model was scaled with a factor of k=0.9 (Small head) and k=1.2 (Large head).

2.2. Experimental demonstration

To confirm the simulation results experimentally, we constructed three birdcage coils: one standard-size (reference) and two extended coils with the same parameters as in the simulations: with copper shield and the slot resonator shown in Fig. 4. The rungs and end-rings of the coils were printed on 0.7-mm-thick RF4 substrates and fixed on foam plastic cylinders with solid plastic holders. Fixed SMD capacitors with a capacitance of 5.6 pF, 5.1 pF, and 4.7 pF respectively were soldered to special gaps in the end-rings between rungs. Additional variable capacitors were placed in parallel with one of the end-ring

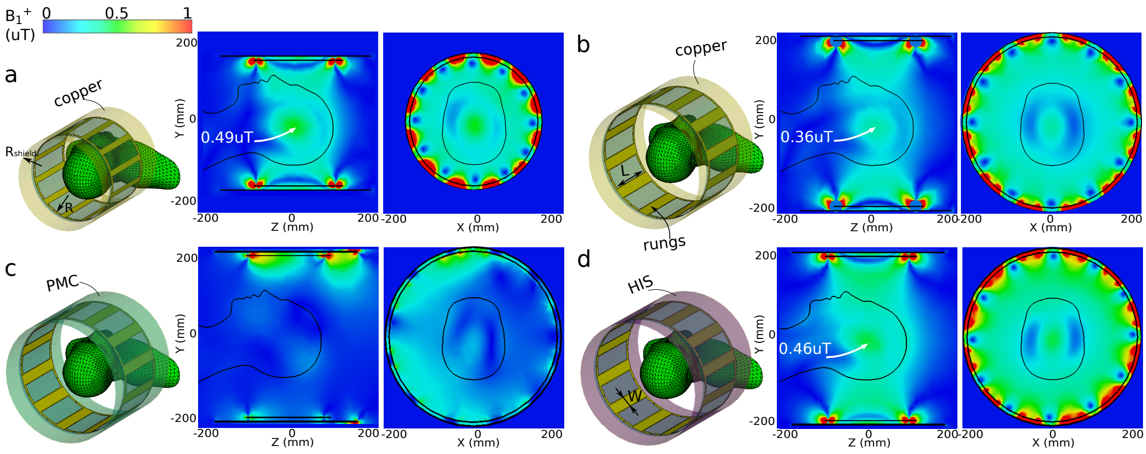

Figure 1: Numerically calculated transmit efficiency distributions with a homogeneous head-shaped phantom (a) reference coil with copper shield (b) extended coil with copper shield (c) extended coil with PMC shield (d) extended coil with HIS shield

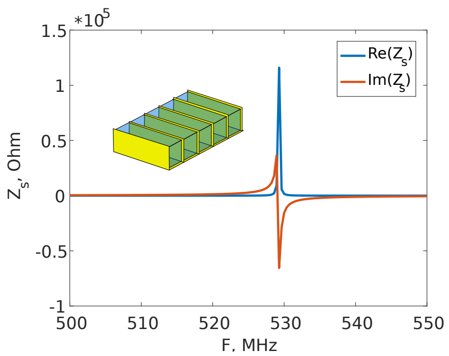

Figure 2: Numerically calculated real and imaginary parts part of the surface impedance of the resonant HIS

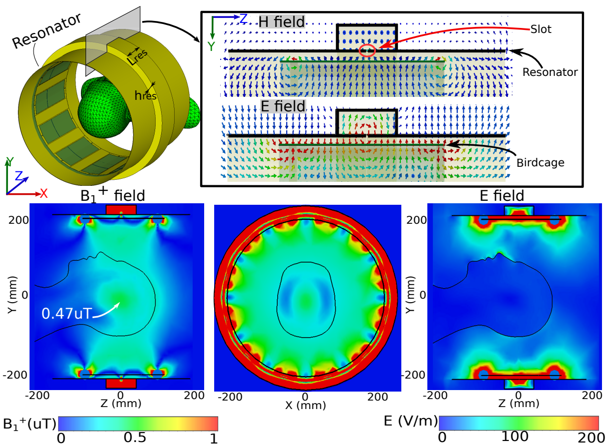

Figure 3: extended coil with resonator: general view, transmit efficiency and E field vector and magnitude distribution

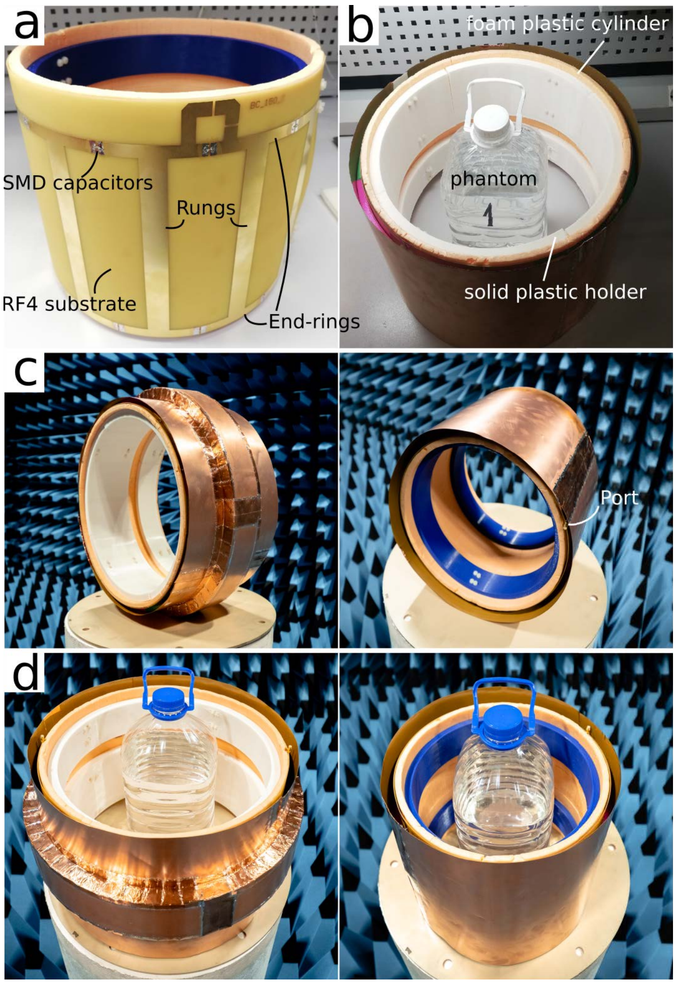

Figure 4: manufactured birdcage coils for experimental comparison (a) birdcage coil of initial size (shown without a shield) (b) extended coil with a copper shield (c) extended coil with cavity-backed slot resonator (left) and reference coil with copper shield (right) (d) the same coils with large phantom within

capacitors 180 degrees apart from the feeding port for fine tuning to the Larmor frequency. The conventional copper shield was built as a solid copper film wrapped around the plastic cylinder and an additional 10-mm-thick plastic holder. To fabricate the slot resonator, we combined a plastic cylinder holder wrapped with copper film with a 1-mm cut in the central transverse plane, and a ring outer coaxial formed by a foam ring metalized by copper film and soldered from outside to ensure shielding action and avoid radiation.

To evaluate the efficiency level vs. the radius of the sample, we made two dielectric phantoms from thin-walled polyethylene cans. The small phantom had a diameter of 9 cm, the big phantom had a diameter of 15 cm. All phantoms were filled with a mixture of water, alcohol, and salt with the same permittivity and conductivity as in the simulations. All coils in the experiments were exited in the linear-polarization regime for simplicity and the transmit efficiency inside the coils was detected by a small pickup-loop probe connected to a port of a vector network analyzer (VNA). The other port of the VNA drives the birdcage at one port. The transmit efficiency proportional to the magnetic field produced by the coil in the center normalized by the square root of the accepted power was determined using the measured S-parameters as $|S_{12}|/\sqrt{1-|S_{11}|^2}/\sqrt{1-|S_{22}|^2}$. Note that the efficiency obtained in this method for the linear polarization is proportional to the efficiency of the same coil driven in the quadrature excitation regime (circular polarization), and thus can be used for comparing the manufactured coils. The efficiency level of the reference tight-fit coil was taken as 100 % for each phantom size in simulations and measurements. To investigate the transmit efficiency distribution inside the phantom of the reference coil and extended coil with the resonator, the transmit efficiency was measured in the XY (transverse) and (YZ) sagittal planes. The efficiency distributions were measured by moving the probe with a programmable 3D positioning system.

3. RESULTS AND DISCUSSION

3.1. Numerical comparison of the transmit and SAR efficiency

3.1.1. Numerical simulations with homogeneous phantom

The transmit efficiency distributions in the longitudinal and transverse planes of a homogeneous head-shaped phantom and the transmit efficiency in its center are shown in Fig. 1 and 3. Fig. 1 (a) and (b) show the results for the reference and extended birdcage coils with the copper shield and the corresponding CST models as insets. As the radius of the coil increases by 30%, its transmit efficiency decreases by 26% as the useful power adsorbed by the sample reduces by 32% (from 0.38 W to 0.26 W for the same accepted power of 0.5 W). Therefore, the increase of the coil is accompanied by additional intrinsic coil losses resulting in lower effibyciency. As it was discussed in [23] one option to increase the efficiency of the birdcage coil is to use an artificial magnetic RF shield instead of a copper one. In the simulations, the copper shield of the extended birdcage coil was replaced with a cylindrical perfect magnetic conductor (PMC) boundary. The result is shown in Fig. 1 (c). As can be seen, the field in the internal volume of the coil becomes strongly inhomogeneous as the wave excited by the port experiences exponential decay while propagating around the circumference of the birdcage instead of producing a standing fundamental mode. This has been previously explained by increased dissipation loss in the sample per unit circumference length [22]. This behavior is non-physical since without natural magnetic conductors achieving infinite surface impedance is possible only at one frequency. Therefore, a more realistic model to predict the properties of the birdcage surrounded by an HIS should use a frequency-dependent surface impedance rather than PMC.

In practice, the in-phase reflection of the electromagnetic waves is provided by thin resonant periodic structures around the resonant frequency. The simulation results for the extended birdcage with a resonant shield modeled by a boundary with properly tuned resonant surface impedance plotted in Fig. 2 are shown in Fig. 1 (d). The presence of the HIS shield enhances the loading of the coil and increases the power dissipated in the phantom back to reference value. From the comparison of Fig. 1 (a) and (d) one may conclude that the extended birdcage in the presence of HIS reaches transmit efficiency just by 6% lower than the reference tight-fit coil (0.46 uT vs. 0.49 uT, accordingly).

Now let us consider the efficiency improvement due to a real resonator. The general view of the extended birdcage coil with the cavity-backed slot, the E- and H-field vector distributions in the cross-section plane of the resonator, transmit efficiency distributions in the sagittal and transverse planes, transmit efficiency and E-field distribution in the sagittal plane are shown in Fig. 3. From the vector distributions, it can be seen that this slot behaves similarly to a ring of magnetic current and adds constructively to the transmit efficiency in the center of the coil (both E- and H-field are increased).

3.1.2. Numerical simulations with voxel human model

In Fig. 5 we show the general views of the reference and extended coils with a copper shield and the extended coil with the cavity-backed slot resonator containing the head of the human voxel model "Duke" used for careful SAR prediction. In the same figure, SAR averaged over 10 g of body tissues and B_1^+ maps in the sagittal plane are shown. It can be seen that the extended coil with a copper shield has the transmit efficiency by 21% lower than the tight-fit coil. However, as the resonator is used as a shield for the extended coil the efficiency recovers and becomes only 5% worse than the reference coil. At the same time, 25% less local SAR is achieved because of lager distance between the coil conductors and the head.

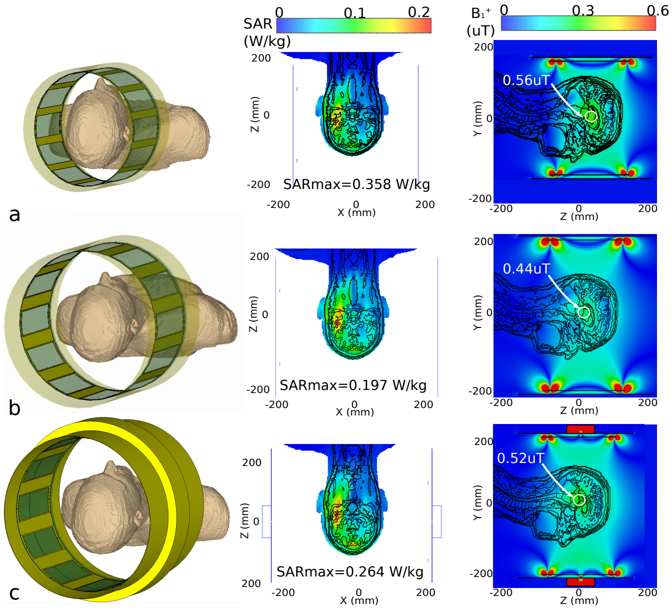

Figure 5: birdcage coil with voxel model of human head: general view (left column), SAR distributions (center column), and transmit efficiency distributions (right column) (a) reference coil with copper shield (b) extended coil with copper shield (c) extended coil with resonator

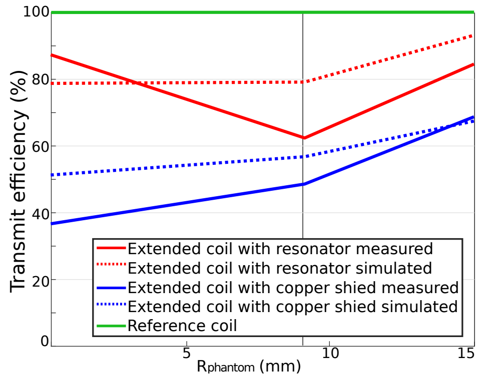

Figure 6: Measured transmit efficiency at the center of a phantom for three sized of the phantom (efficiency of the reference coil was taken as 100% level).

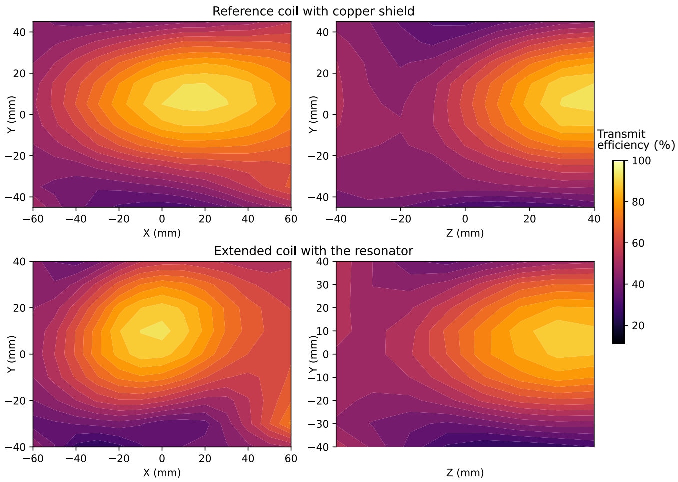

Figure 7: Measured map of normalized transmit efficiency inside the phantom for the reference coil and extended coil with the resonator in XY and YZ plane

Table 1 summarizes the simulation results of the reference and extended coils with a copper shield and the extended coil with the resonator. The table includes the results obtained using three voxel models scaled in sizes, with different factors. It can be seen for all head sizes, the SAR for the extended birdcage coil with the resonator is lower than for the reference coil and the transmit efficiency is higher than for the extended coil with the copper shield. A SAR efficiency, the most important figure of merit of transmit MRI coils, was defined as $B_1^+/\sqrt{\text{SAR}}$. It can be seen from the table that for average-size and large-size head, the SAR efficiency in the presence of the resonator is higher than for the copper shield for the same extended coil size, while for the small-sized head it is comparable.

3.2. Experimental confirmation

To confirm the numerical simulations, we constructed three birdcage coils: the reference coil with a copper shield, the extended coil with a copper shield, and extended coil with the cavity-backed slot resonator, and evaluated them on a bench.

The graph in Fig. 6 shows the dependence of the transmit efficiency at the center of the phantom compared to one of the reference coil for three phantom sizes. Although the efficiency of the extended coil with the resonator cannot recover the level of the reference coil, the measured transmit efficiency of the extended coil with the resonator is from 10 to 40% higher than for the extended coil with a copper shield depending on the sample size. In Fig. 6 the measured values are compared to the simulation results. A qualitative comparison of the dependencies can be observed. The deviations between the simulations and measurements could be explained by differences in the phantom shape and position of the phantom and probe inside the coil.

In Fig. 7 color maps of the measured efficiency inside the large phantom in XY and YZ planes for the reference coil and extended coil with the resonator. It can be seen that as was expected from the simulations, the two coils have the similar transmit efficiency pattern shapes inside the phantom.

4. Conclusions

In this work, a new application of an artificial magnetic shield in clinical MRI of a human head at 7 T was proposed. It was shown by numerical simulations that the transmit efficiency of the birdcage coil depends on its size and the best efficiency can be achieved when all transmit power is dissipated in the phantom. When extended the coil becomes less efficiency a considerable part of the

Table 1: Numerical comparison of the transmit efficiency and SAR.

		Small head	Average-size	Large head
Reference coil	B_1^+, uT	0.59	0.56	0.43
	SAR, W/kg	0.36	0.358	0.26
	$B_1^+/\sqrt{SAR}$, uT/$\sqrt{W/kg}$	**0.98**	**0.96**	**0.84**
Extended coil	B_1^+, uT	0.45	0.44	0.4
	SAR, W/kg	0.19	0.197	0.22
	$B_1^+/\sqrt{SAR}$, uT/$\sqrt{W/kg}$	**1**	**0.99**	**0.85**
Extended coil with resonator	B_1^+, uT	0.51	0.52	0.4
	SAR, W/kg	0.264	0.264	0.21
	$B_1^+/\sqrt{SAR}$, uT/$\sqrt{W/kg}$	**0.99**	**1.01**	**0.88**

transmit power is lost inside the coil. Therefore, the extended coil with a conventional shield though more comfortable for the patient is by 20-40% less efficient than the initial tight-fit coil. However, we have shown that in this case the transmit efficiency can be again increased by changing the copper shield to an artificial magnetic shield. We have experimentally shown that the proposed slot resonator backed by a coaxial cavity increases the transmit efficiency of the extended birdcage by 10-40% depending on the sample size in comparison to a copper shield. It allows the extended coil to be only 10% less efficient than a tight-fit reference coil. At the same time, the maximum local SAR value of the proposed coil is 25% lower than for the reference coil due to an enlarged distance between the conductors and the head. The SAR efficiency of the proposed coil is even 3% better than of the reference one.

Therefore, due to the in-phase interference between the field of the extended birdcage and the cavity-backed slot, due to extended size the proposed coil is more comfortable for the patient than the reference one, at the expense of 5-10% efficiency reduction, but showed the same or better SAR performance. The constructive interference effect was confirmed by a comparison to an ideal HIS shield in simulations showed the same effect on the coil's efficiency. In both cases the part of the accepted transmit power which is absorbed by the sample and not lost in the coil increases.

The presence of the resonator enhanced the transmit efficiency of the extended coil for all considered sizes of the sample. The efficiency gain depends on the phantom size: the smaller the sample the larger the gain due to the resonator. Finally, as clearly follows from simulations and measurements, the resonator does not negatively affect the transmit efficiency distribution inside a phantom, therefore does not change homogeneity of images.

Thought the proposed resonator is just a single slot which behaves with respect to the volume of the coil as a ring of magnetic current, its effect on the efficiency is the same as of a HIS cylindrical boundary. On the HIS boundary an azimuthally flowing surface magnetic current distributed along the axial direction is induced. Despite a periodic corrugated structure would better approximate this distribution, the proposed single-slot resonator is easy to build without any high-perimittivity materials. Therefore, the proposed resonator was found to be a very interesting alternative to conventional copper shields of birdcage coils for human brain imaging at 7 T, which enables efficient operation with increased free space for the patient.

5. acknowledgments

This work was supported by the Russian Science Foundation (Grant No. 18-19-00482). The authors thank Georgiy Solomakha for his help and useful discussions.

References

[1] A. G. Webb (Ed.), Magnetic resonance technology: hardware and system component design, Royal society of chemistry, Cambridge, UK, 2016.

[2] J. T. Vaughan, J. R. Griffiths, RF Coils for MRI, A John Wiley and Sons, 2012.

[3] E. Hayes, The development of the birdcage resonator: a historical perspective, NMR in Biomedicine 22(9) (2009) 908–18.

[4] F. D. Doty, G. Entzminger, J. Kulkarni, K. Pamarthy, J. P. Staab, Pros and cons of ultra-high-field MRI/MRS for human application, Progress in Nuclear Magnetic Resonance Spectroscopy 109 (2018) 1–50.

[5] R. Pohmann, O. Speck, K. Scheffler, Signal-to-noise ratio and MR tissue parameters in human brain imaging at 3,4, and 9.4 Tesla using current receive coil arrays, Magnetic Resonance in Medicine 75. doi:10.1002/mrm.25677.

[6] B. Guerin, J. Villena, A. Polimeridis, E. Adalsteinsson, L. Daniel, J. White, L. Wald, The ultimate signal-to-noise ratio in realistic body models, Magnetic Resonance in Medicine 78. doi:10.1002/mrm.26564.

[7] E. Moser, E. Laistler, F. Schmitt, G. Kontaxis, Ultra-high field NMR and MRI—the role of magnet technology to increase sensitivity and specificity, Frontiers in Physics 5 (2017) 33.

[8] J. Vaughan, M. Garwood, C. Collins, W. Liu, L. DelaBarre, G. Adriany, P. Andersen, H. Merkle, R. Goebel, M. Smith, K. Ugurbil, 7T vs. 4T: RF power, homogeneity, and signal-to-noise comparison in head images, Magnetic resonance in medicine : official journal of the Society of Magnetic Resonance in Medicine / Society of Magnetic Resonance in Medicine 46 (2001) 24–30. doi:10.1002/mrm.1156.

[9] N. Avdievich, Transceiver-phased arrays for human brain studies at 7 T, Applied Magnetic Resonance 41 (2-4) (2011) 483–506.

[10] N. Avdievich, G. Solomakha, L. Ruhm, J. Bause, K. Scheffler, A. Henning, Bent folded-end dipole head array for ultrahigh-field MRI turns "dielectric resonance" from an enemy to a friend, Magnetic resonance in medicinedoi:10.1002/mrm.28336.

[11] P. F, H. J. Beqiri A and, M. SJ., Parallel transmission for ultrahigh-field imaging, NMR Biomed 29(9) (2016) 1145–1161.

[12] J. Hoffmann, S. Gunamony, K. Scheffler, R. Pohmann, Numerical and experimental evaluation of RF shimming in the human brain at 9.4 T using a dual-row transmit array, Magma (New York, N.Y.) 27. doi:10.1007/s10334-013-0419-y.

[13] F. D. Doty, G. Entzminger, J. Kulkarni, K. Pamarthy, J. P. Staab, Radio frequency coil technology for small-animal MRI, NMR Biomed 20 (2007) 304–325.

[14] M. D. Harpen, Radiative losses of a birdcage resonator, Magn Reson Med 29 (1993) 713–716.

[15] C. M. Collins, S. Li, Q. X. Yang, M. B. Smith, A method for accurate calculation of B_1 fields in three dimensions. Effects of shield geometry on field strength and homogeneity in the birdcage coil, J. Magn. Res. 125(2) (1997) 233–241.

[16] F. Capolino, Theory and Phenomena of Metamaterials, Taylor and Francis Group, 2009.

[17] D. Sievenpiper, L. Zhang, R. J. Broas, N. Alexöpolous, E. Yablonovitch, High-impedance electromagnetic surfaces with a forbidden frequency band, IEEE Trans. Microw. Theory Tech 47(11) (1999) 2059–2074.

[18] A. Feresidis, G. Goussetis, S. Wang, J. Vardaxoglou, Artificial magnetic conductor surfaces and their application to low-profile high-gain planar antennas, IEEE Trans. Ant. Propag. 53(1) (2005) 209–215.

[19] P. Kildal, Artificially soft and hard surfaces in electromagnetics, IEEE Trans. Ant. Propag. 8(10) (1990) 1537–1544.

[20] Z. Chen, K. Solbach, D. Erni, A. Rennings, Electromagnetic field analysis of a dipole coil element with surface impedance characterized shielding plate for 7-T MRI, IEEE Trans. Microw. Theory Tech 64(3) (2016) 392–395.

[21] Z. Chen, K. Solbach, D. Erni, A. Rennings, Improving B_1 efficiency and signal-to-noise-ratio of a surface coil by a high-impedance-surface RF shield for 7-T magnetic resonance imaging, IEEE Trans. Micr. Theor. Tech. 65(3) (2017) 988–997.

[22] C. van Leeuwen, M. Lunenburg, S. Glybovski, P. Luijten, D. Klomp, C. van den Berg, A. Raaijmakers, Improved performance of birdcage coils using a split-ring resonator magnetic shield, In Proceedings of Joint Annual Meeting ISMRM – ESMRMB.

[23] K. Lezhennikova, R. Abdeddaim, A. Hurshkainen, A. Vignaud, M. Dubois, P. Jomin, D. Berrahou, A. Raaijmakers, N. Avdievich, I. Melchakova, S. Enoch, P. Belov, C. Simovski, S. Glybovski, Constructive near-field interference effect in a birdcage MRI coil with an artificial magnetic shield, Phys. Rev. Applied 13 (2020) 064004. doi:10.1103/PhysRevApplied.13.064004.

[24] Q. X. Yang, J. Wang, C. M. Collins, M. B. Smith, X. Zhang, K. Ugurbil, W. Chen, Phantom design method for high-field MRI human systems, Magn Reson Med. 52(5) (2004) 1016–1020.

[25] A. Christ, W. Kainz, E. Hahn, K. Honegger, M. Zefferer, E. Neufeld, W. Rascher, R. Janka, W. Bautz, J. Chen, B. Kiefer, P. Schmitt, H.-P. Hollenbach, J. Shen, M. Oberle, D. Szczerba, A. Kam, J. Guag, N. Kuster, The virtual family-development of surface-based anatomical models of two adults and two children for dosimetric simulations, Physics in Medicine and Biology 55 (2010) N23–38. doi:10.1088/0031-9155/55/2/N01.